THE JOURNAL OF PHYSICAL CHEMISTRY Letters

Letter

pubs.acs.org/JPCL

Bringing Far-Field Subdiffraction Optical Imaging to Electronically Coupled Optoelectronic Molecular Materials Using Their Endogenous Chromophores

Samuel B. Penwell,[†] Lucas D. S. Ginsberg,[†] and Naomi S. Ginsberg*[,†,‡,§,∥,⊥]

[†]Department of Chemistry and [‡]Department of Physics, University of California, Berkeley, California 94720, United States

[§]Physical Biosciences and [∥]Materials Sciences Divisions, Lawrence Berkeley National Laboratory, Berkeley, California 94720, United States

[⊥]Kavli Energy NanoSciences Institute, Berkeley, California 94720, United States

Supporting Information

ABSTRACT: We demonstrate that subdiffraction resolution can be achieved in fluorescence imaging of functional materials with densely packed, endogenous, electronically coupled chromophores by modifying stimulated emission depletion (STED) microscopy. This class of chromophores is not generally compatible with STED imaging due to strong two-photon absorption cross sections. Yet, we achieve 90 nm resolution and high contrast in images of clusters of conjugated polymer polyphenylenevinylene-derivative nanoparticles by modulating the excitation intensity in the material. This newfound capability has the potential to significantly broaden the range of fluorophores that can be employed in super-resolution fluorescence imaging. Moreover, solution-processed optoelectronics and photosynthetic or other naturally luminescent biomaterials exhibit complex energy and charge transport characteristics and luminescence variations in response to nanoscale heterogeneity in their complex, physical structures. Our discovery will furthermore transform the current understanding of these materials' structure−function relationships that have until now made them notoriously challenging to characterize on their native, subdiffraction scales.

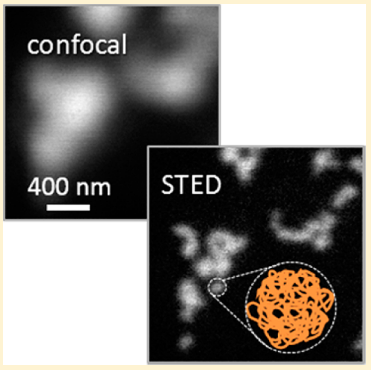

Many complex, naturally luminescent materials possess nanoscale structural heterogeneity. The effect of this heterogeneity on their optical properties has been difficult to determine because of the challenges of imaging naturally luminescent materials below the optical diffraction limit. In many cases these materials are composed of organic molecular chromophores that are packed so densely that they are electronically coupled—their Coulomb interactions rediagonalize their electronic quantum mechanical states, leading to optical properties of the resulting material that differ significantly from those of the individual molecular components.[1] These properties range from static spectral characteristics and oscillator strengths to the ultrafast dynamics of charge carrier or excitation energy transport.[2−6] For example, in printable electronics although the low cost and ease of manufacture of low-temperature solution-processing are highly attractive, the resulting drying-mediated kinetically trapped solid structures must be understood in the context of their local and macroscopic effects on the functional electronic and optical properties of these materials.[7−13] When the morphology of these materials is critical to their function, fluorescent labeling, as is performed in bioimaging, is impractical because it disrupts the very structure whose effects are meant to be studied. Furthermore, the luminescence of the endogenous chromophores can swamp that of the dilute labels, and the labels may also electronically couple to the material, perturbing the function of both. These challenges exist for organic semiconducting solids composed of small π-conjugated molecules and polymers used in optoelectronic applications, and they are equally problematic in luminescent biomaterials with endogenous chromophores, as found in photosynthesis,[14] circadian rhythm regulation,[15] and other forms of bioluminescence.[16] A common challenge in characterizing heterogeneous, naturally luminescent materials is that there are no straightforward means to obtain their optical properties on the characteristic length scale over which they vary.

Far-field super-resolution fluorescence imaging has become very prominent, in particular in bioimaging, where molecules of interest are fluorescently labeled so that their nanoscale organization can be determined. Whether employing structured illumination microscopy,[17] stochastic photoactivated approaches,[18−21] or stimulated emission depletion (STED) imaging,[22] care is generally taken in selecting the fluorescent labels used. In particular, in STED microscopy, though some efforts employ luminescent inorganic nanoparticles,[23−27] the fluorescent labels are typically small and rigid π-conjugated dye

Received: June 6, 2015
Accepted: June 29, 2015

DOI: 10.1021/acs.jpclett.5b01200
J. Phys. Chem. Lett. 2015, 6, 2767−2772

molecules that are comparatively resistant to photobleaching and that have been selected based on whether their photophysical properties are empirically found to be compatible with stimulated emission depletion.[28,29] Fluorophores with high triplet, photoisomerization, or other photochemistry yields, fluorophores prone to photodamage, and especially fluorophores that permit absorption of the annular STED quenching laser wavelength on account of a limited Stokes shift or lingering red absorption tail are generally incompatible with STED microscopy. In addition to linear absorption of the STED laser pulse, two-photon absorption (2PA), which is a prominent second-order process in π-conjugated organic molecules[30,31] and solid materials,[32] can also prevent appropriate levels of stimulated emission depletion. STED microscopy employs considerable laser intensities to induce adequate stimulated emission, yet it is precisely at these high intensities that 2PA can become a competing factor that may dominate the stimulated emission process.[33,34] Moreover, the inflexibility of working with endogenous chromophores in naturally luminescent materials and the requirements for well-behaved fluorescent labels in super-resolution imaging together present severe challenges toward optically characterizing naturally luminescent materials on the nanoscale.

In spite of these challenges, here, we demonstrate that subdiffraction resolution in STED microscopy can be achieved on materials with endogenous, electronically coupled chromophores. We image luminescent conjugated polymer nanoparticles with 90 nm resolution. One important adaption that we employ to circumvent 2PA-induced fluorescence from the STED laser pulse is an excitation intensity modulation scheme.[35,36] We envision that this advance will open up the possibility to employ previously discarded labels in bioimaging. It will also importantly enable direct imaging of solution-processed luminescent optoelectronic materials on the subdiffraction scales characteristic of their structural heterogeneities, which can disproportionately determine the limits on their functionality.

In this study, we focus on polyphenylenevinylene derivative poly(2,5-di(hexyloxy)cyanoterephthalylidene) (CN-PPV) solids, prepared as nanoparticles.[37] Each CN-PPV particle is composed of one or more aggregated polymer chains. As shown in Figure 1a, in the solid phase, CN-PPV has a broad absorption spectrum, extending from the ultraviolet to a peak absorption wavelength at 480 nm, and tailing off around 600 nm. Its fluorescence is peaked around 625 nm. We therefore use wavelengths of 540 nm for the excitation laser pulse and 740 nm for STED depletion. We find that 2PA at the STED laser pulse wavelength indeed occurs, as evidenced by a superlinear power dependence in the low power limit (Supporting Information Figure S1). Furthermore, we measure 2PA-induced fluorescence in our 610−640 nm imaging detection window, ∼300 meV higher in energy that the STED laser photons (Figure 1a). The material's electronic energy levels and corresponding transitions that are relevant to performing STED microscopy are presented in Figure 1b. The excitation laser (green) couples the ground and excited states in a diffraction-limited spot; the STED laser (red) drives an electronic transition on the Stokes-shifted line to deplete the excited state in a spatially dependent manner to achieve super-resolution[22] (see below). Also illustrated is the 2PA of the STED photons whose excitations presumably thermalize to the same excited state as those generated through linear resonant absorption of the excitation laser. The time-resolved

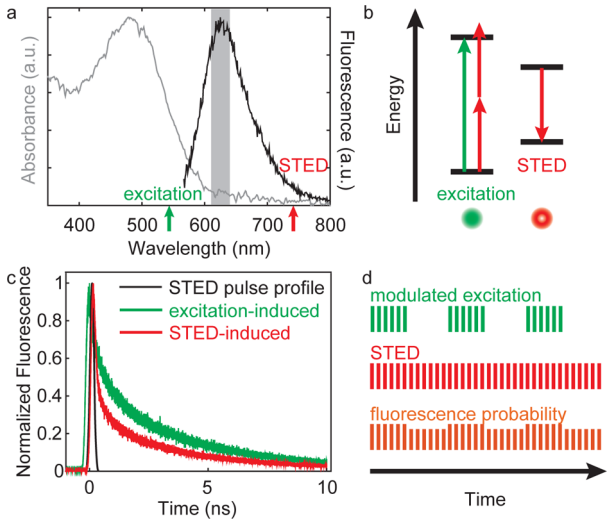

Figure 1. Experimental scheme. (a) CN-PPV solid absorbance and fluorescence emission spectra. Green and red arrows indicate excitation and STED laser wavelengths, respectively. The shaded band indicates the bandwidth of fluorescence collection. (b) CN-PPV energy level diagram. After resonant excitation (green) and vibrational relaxation, the STED laser (red) induces stimulated emission on the Stokes-shifted line. 2PA of the STED laser wavelength is also indicated. (c) Time-resolved fluorescence of CN-PPV solids induced by excitation pulse (green) and by STED pulse (red). The black curve is a sketch of the approximate timing and duration of the STED pulse arrival. (d) Timing diagram showing modulated excitation pulse train (green), unmodulated STED pulse train (red), and modulated CN-PPV fluorescence probability (orange).

fluorescence of the CN-PPV is depicted in Figure 1c, along with the STED laser pulse temporal profile (black curve). When induced by the excitation laser at 540 nm (green), the transient follows a typical biexponential fluorescence decay.[38] More unusually, when induced by the STED laser pulse at 740 nm (red), the fluorescence intensity rises abruptly with the onset of the nonlinear 2PA and then also falls abruptly with the onset of stimulated emission. The shape of this decay curve primarily depends on the time-dependent competition between 2PA and stimulated emission,[33] as mirrored in simulations of the system (Supporting Information Figure S2).

To image solids of CN-PPV, we modify traditional STED microscopy in an apparatus (Supporting Information Figure S3) that includes a home-built epifluorescence microscope. We excite the samples with a pulse energy of 0.16 pJ, and we follow this few-picosecond, diffraction-limited excitation with a ∼120 ps duration, 570 pJ, annular Laguerre−Gauss-mode STED pulse (Figure 1b) tuned to the red of the CN-PPV fluorescence emission peak in order to stimulate emission everywhere but in the subdiffraction center of the original excitation spot via nonlinear saturation. Because we operate the microscope with noncollinear parametric amplifiers pumped with a 200 kHz repetition rate ultrafast regenerative amplifier, we are able to carefully tune, control, and optimize many experimental parameters, including pulse wavelengths, bandwidths, durations, and relative delays. Also, by contrast with common STED microscopes, to eliminate the effects of absorption of the STED laser, we modulate the excitation pulse intensity at 500 Hz and separately record on a single photon avalanche diode (SPAD) the fluorescence counts during the "excitation-on" and "excitation−off" phases of the modulation cycle (Figure 1d). This modulation scheme enables us to specifically select for

DOI: 10.1021/acs.jpclett.5b01200
J. Phys. Chem. Lett. 2015, 6, 2767−2772

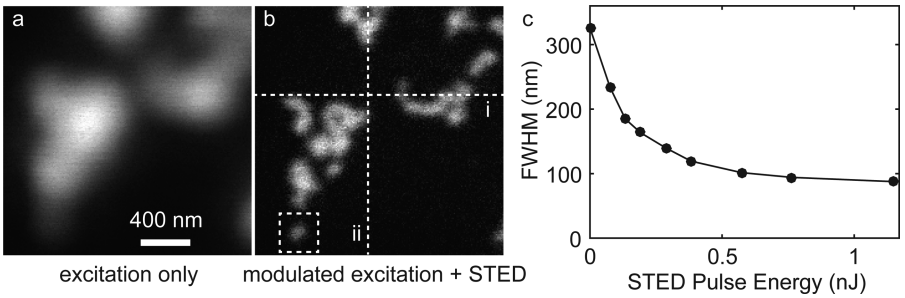

Figure 2. Modulated STED imaging of conjugated polymer nanoparticles. (a) Standard fluorescence image. (b) STED image of same region of interest as in panel a, employing time gating and excitation pulse modulation. A linear gray scale is used in each of panels a and b, scaled to span from zero to the maximum intensity in each panel. Line scans at the positions indicated with dashed lines are plotted in Figure 3. (c) Full width at half-maximum (fwhm) of Gaussian fits to the nanoparticle feature boxed in panel b under time-gated and excitation-modulated STED imaging as a function of STED laser pulse energy.

fluorescence induced by the modulated excitation pulse when forming an image in order to obtain superior contrast. Last, time-gated detection has been used to improve spatial resolution by eliminating fluorescence collection from the diffraction-limited excitation volume prior to the onset of stimulated emission.[39,40] Here, our time-gated detection, with an extremely rapid 200 ps turn-on time,[41,42] furthermore eliminates early time fluorescence induced by the diffraction-limited excitation and STED pulses.

Using the above scheme, we image clusters of nanoparticles composed of solution-processed CN-PPV. The images in Figure 2a–b reveal that our adaptation of STED microscopy successfully addresses the challenges of 2PA of the STED laser. Using the excitation pulse only (Figure 2a), the particles within individual clusters are not at all resolved, whereas the addition of the time-gated STED pulse, along with excitation modulation, reveals multiple features within each cluster with an approximately 3-fold improvement in resolution (Figure 2b). Even with time gating, without the excitation modulation, the background intensity is both higher and nonuniform (Supporting Information Figure S4). This deficiency occurs because 2PA-induced fluorescence due to the roughly micron-sized STED laser spot cannot be distinguished from the desired unquenched excitation-pulse-induced fluorescence originating in the subdiffraction volume centered on the null of the STED laser's Laguerre–Gauss mode. We also established the dependence of the spatial resolution on the STED pulse intensity (Figure 2c) by imaging the individual bead boxed in the bottom left corner of Figure 2b at multiple STED laser intensities and by measuring and plotting the width of the nanoparticle feature in these successive measurements. Similar to typical STED experiments,[43] the feature size drops and then saturates at ~90 nm.

To analyze the impact that modulating the excitation pulse has on image formation and quality, we present in Figure 3 line scans across the STED image of the nanoparticles in Figure 2b (black) and compare them to the corresponding line scans obtained without modulation (gray). The locations of these line scans are indicated with dashed lines enumerated i and ii in Figure 2b. Because, at the 500 Hz modulation frequency, we separately record the fluorescence counts at a given pixel while the excitation pulse illuminates the sample and while it does not, the gray traces in Figure 3 are straightforward to extract from the data set that generates a modulated STED image (see Experimental Methods and Supporting Information Figure S4). The unmodulated gray trace in Figure 3a (scan i in Figure 2b)

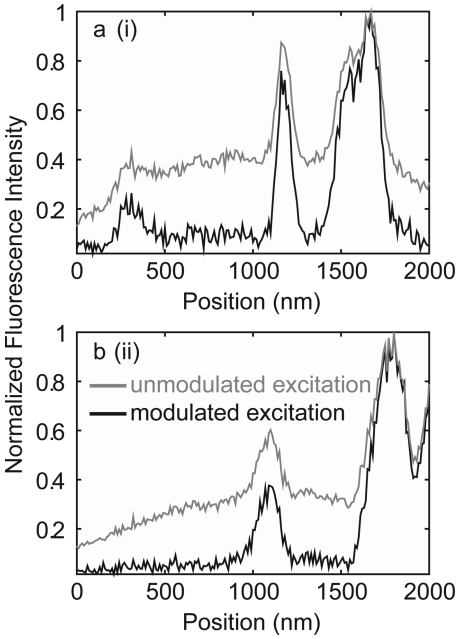

Figure 3. Line scans of the STED image in Figure 2b. Line scans (a) and (b) correspond to the intensity profiles measured on the dashed lines labeled i and ii, respectively, in Figure 2b. In each case, the black trace corresponds directly to the intensity in the excitation-modulated STED image in Figure 2b. The gray traces correspond to the intensity detected during "excitation on" periods only, as though there is no excitation modulation. The traces represent averages over three adjacent rows of pixels.

shows an apparent rise to a plateau around 200 nm, whereas only the modulated (black) trace shows that there is an isolated feature centered at ~300 nm. Overall, the unmodulated "baseline" of detected STED-induced fluorescence is not uniform, making it impossible to quantitatively compare features to one another. Figure 3b (scan ii in Figure 2b) reveals an unmodulated baseline amplitude greater than the size of the feature at ~1100 nm riding on top of it. Furthermore, the relative extent of the dip between the two features at the far right appears significantly deeper in the unmodulated gray trace than in the modulated trace. In both cases, the nonuniform unmodulated background levels represent imaging artifacts that, without the ability to compare to the modulated line scans, can be mistaken for features themselves or can distort the relative size of real features. These imaging artifacts arise because the unmodulated, STED-induced fluorescence background level at

DOI: 10.1021/acs.jpclett.5b01200
J. Phys. Chem. Lett. 2015, 6, 2767–2772

any given pixel is proportional to the density of other nanoparticles illuminated by the off-axis portion of the large (>1 μm diameter) transverse mode of the STED laser pulse[27] (Supporting Information Figures S4 and S5a). Clearly, without excitation modulation the ability to resolve small features is also heavily compromised.

The modulated STED image in Figure 2b illustrates the ability to perform super-resolved far-field fluorescence imaging on materials with densely packed endogenous chromophores that have not previously been accessible in this way. Furthermore, when imaging a material that is able to fluoresce as a result of STED illumination alone, modulating the excitation pulse significantly improves the image contrast. To explain how and why we have successfully super-resolved materials with photophysical properties that are generally considered to be nonideal for STED microscopy, we discuss the physics underlying the contrast and resolution that we have achieved. First, we consider the increased complexity of STED imaging specifically using organic chromophores for which nonlinear 2PA competes with linear stimulated emission at the STED laser pulse wavelength. Our results reveal that the time dependence of the competition of these two processes with different intensity dependences can limit the effects of 2PA. In other words, the STED pulse temporal profile ensures that stimulated emission can persist at intensities at which 2PA is waning in order to quench a significant fraction of the 2PA-induced fluorescence, as illustrated in Figure 1d. The monotonically decreasing and saturating behavior of the resolution curve obtained in Figure 2c also demonstrates that stimulated emission still dominates 2PA even at the highest peak pulse intensities. Because this quenching of 2PA-induced fluorescence occurs over and is limited to the course of the ~120 ps STED pulse duration, fast gated detection on a similar time scale[41,42] enables us to suppress a significant fraction of 2PA-induced fluorescent photons from being detected. Although the line scans in Figure 3 illustrate that even gated detection is imperfect, our straightforward excitation pulse modulation further selects for fluorescence induced by the excitation pulse only, in order to significantly improve image contrast.

The minimum CN-PPV nanoparticle feature size of 90 nm that we have observed at a maximum STED intensity in Figure 2c could be limited by the excitation modulation rate, sample heating, possible exciton annihilation effects,[44] an imperfect null in the Laguerre−Gauss mode of the STED pulse, or by the inherent spatial resolution of the microscope (Supporting Information Figure S5b). For nanoparticles larger than the typical exciton diffusion lengths of several nanometers measured in related PPV materials[45−47] it is possible that the electronic coupling in the material also limits the ultimate resolution. Additional temporal stretching of the STED pulse to decrease its peak intensity could further mitigate 2PA and enable higher fluences and potentially higher spatial resolution to be achieved. Nevertheless, the ability to image heterogeneities in solution-cast, functional optoelectronic materials using their endogenous chromophores even at the scale of ~100 nm will be of significant utility because many of their features that are smeared out at the diffraction limit are able to be resolved on this subdiffraction scale.

In sum, we have demonstrated that it is possible to perform subdiffraction STED fluorescence imaging of electronically coupled materials as a result of and in spite of their densely packed endogenous chromophores. We have shown that excitation modulation aids in eliminating the challenges of STED laser 2PA, and we anticipate that our findings can be generalized to the large class of organic chromophores that exhibit 2PA so that STED imaging may be performed on a much wider range of materials than originally demonstrated or anticipated. These materials could include dyes not currently considered to be compatible with STED or other super-resolution fluorescence approaches, photosynthetic membranes, or other autofluorescent biomaterials. In fact, the extremely bright conjugated polymer nanoparticles employed in this study could even be used as labels in super-resolution imaging applications. Moreover, our findings open up the possibility to image the subdiffraction heterogeneities in solution-processed solid optoelectronic materials composed of π-conjugated molecules or even of colloidal nanocrystals. This avenue could reveal directly how these heterogeneities not only affect such a material's local optical properties but also how they affect the material's macroscopic electronic properties that determine its functional potential. Last, although 2PA could be reduced by increasing the duration of the STED laser pulse, our shorter pulse duration and similarly fast gated detection could enable schemes to resolve ultrafast energy transport[48,49] in similar electronically coupled materials on the nanometer scales that no longer average over their heterogeneities. Such a scheme would be a significant improvement over bulk approaches used to measure exciton migration[50−54] that cannot currently explain which trajectories an excitation might favor as a function of specific features of the film morphology.

EXPERIMENTAL METHODS

Sample Preparation and Characterization. A ~0.005% (w/v) solution of CN-PPV in tetrahydrofuran (THF) was made in a nitrogen glovebox. A 0.2 mL aliquot of the 0.005% CN-PPV in THF solution was quickly added to 0.8 mL of ultrapure water while the water was ultrasonicated. This solution was drop cast onto coverslips and allowed to dry overnight in air. Once dry, residual oxygen and water was removed from the sample in the antechamber of a nitrogen glovebox and the samples were then encapsulated in the glovebox using UV cure epoxy (EPO-TEK, OG159-2). A representative absorbance spectrum of a CN-PPV film was acquired with a UV−vis spectrophotometer (Agilent Cary 100); fluorescence spectra of CN-PPV nanoparticles encapsulated on a glass slide were obtained with a Horiba Fluoromax-4 fluorimeter at an excitation wavelength of 540 nm. *Imaging*. Images were obtained in a home-built epifluorescence microscope with a 63× 1.4NA Plan Apo Leica objective (HC PL APO 63*x*/1.40 oil CS2, Leica Material #11506350). The excitation and STED laser pulse trains at 200 kHz were derived from third-harmonic and second-harmonic noncollinear optical parameteric amplifiers (NOPA) (Light Conversion), respectively, pumped by a 10 W Light Conversion PHAROS regeneratively amplified laser system with a fundamental wavelength of 1030 nm. The 0.16 pJ excitation pulse was centered at 540 nm, and the 570 pJ STED pulse was centered at 740 nm with a bandwidth set to 12 nm. Excitation and STED pulse delays, spatial modes, energies, and polarizations are prepared prior to cofocusing the pulses in the microscope (see Supporting Information Figure S3 for additional details). The sample is rastered with a PI Nano scanning piezo stage (P-545.3C7) in steps of 10 nm over a 2 μm × 2 μm area with a dwell time of 50 ms/pixel to form an image. At each pixel, epifluorescence is collected between 610 and 640 nm through our dichroics (Chroma T650spxr and T600lpxr-UF2) and two

DOI: 10.1021/acs.jpclett.5b01200
J. Phys. Chem. Lett. 2015, 6, 2767−2772

emission filters (Chroma ET625/30m) and focused onto a fast gated SPAD detector with a 200 ps rise time (Prof. Alberto Tosi, SPAD lab, Politecnico di Milano; PicoQuant) controlled by a Picosecond Delayer (MPD) to eliminate prompt fluorescence. We phase lock the detection to the optical chopper cycle and separately accumulate the photon count rates during the corresponding "excitation on" and "excitation off" phases for multiple cycles. The count rates obtained during the open and closed cycles of the chopper are each corrected for the classic pile-up effect with a simple Poisson correction factor (see Supporting Information) before we take the difference of the two to isolate the count rate that is attributed to the modulated excitation pulse only.

Fluorescence lifetime measurements were performed in the microscope with the fast-gated SPAD using a HydraHarp 400 (PicoQuant) using an excitation pulse energy of 0.22 pJ or a STED pulse energy of 370 pJ.

■ ASSOCIATED CONTENT

Supporting Information

The Supporting Information contains a STED-induced fluorescence power dependence, simulated time-resolved fluorescence traces, an experimental schematic, a comparison of nanoparticle images with either excitation or STED laser pulses and with both excitation and STED laser pulses, with and without excitation modulation, measured point spread functions for excitation and STED pulses, and a supplement to the experimental methods on signal recovery. The Supporting Information is available free of charge on the ACS Publications website at DOI: 10.1021/acs.jpclett.5b01200.

■ AUTHOR INFORMATION

Corresponding Author

*E-mail: nsginsberg@berkeley.edu.

Author Contributions

S.B.P., L.D.S.G., and N.S.G. designed the research. S.B.P. and L.D.S.G. constructed the apparatus and characterized the point spread functions. L.D.S.G. prepared the samples. S.B.P performed the imaging and simulated the experiment. N.S.G. supervised the project. S.B.P. and N.S.G. wrote the manuscript and all authors revised and approved the manuscript.

Notes

The authors declare no competing financial interest.

■ ACKNOWLEDGMENTS

This work has been supported by a David and Lucile Packard Fellowship for Science and Engineering to N.S.G. and by The Dow Chemical Company under contract #244699. We thank A. Tosi and M. Buttafava of SPAD lab, Politecnico di Milano, for discussions and the generous trial of the fast-gated SPAD and N. Bertone and PicoQuant GmbH for providing a demo of the HydraHarp400 photon counting apparatus. We thank D. M. Neumark for the use of a grating stretcher. S.B.P. acknowledges a Department of Energy Graduate Research Fellowship (contract no. DE-AC05-060R23100) and N.S.G. acknowledges an Alfred P. Sloan Research Fellowship.

■ REFERENCES

(1) Pope, M.; Swenberg, C. E. *Electronic Processes in Organic Crystals and Polymers*; Oxford University Press: New York, 1999.

(2) Scholes, G. D. Long-Range Resonance Energy Transfer in Molecular Systems. *Annu. Rev. Phys. Chem.* **2003**, *54*, 57−87.

(3) Brédas, J.-L.; Beljonne, D.; Coropceanu, V.; Cornil, J. Charge-Transfer and Energy-Transfer Processes in Pi-Conjugated Oligomers and Polymers: A Molecular Picture. *Chem. Rev.* **2004**, *104*, 4971−5004.

(4) Scholes, G. D.; Rumbles, G. Excitons in Nanoscale Systems. *Nat. Mater.* **2006**, *5*, 683−696.

(5) Spano, F. C. Excitons in Conjugated Oligomer Aggregates, Films, and Crystals. *Annu. Rev. Phys. Chem.* **2006**, *57*, 217−243.

(6) Clark, J.; Silva, C.; Friend, R. H.; Spano, F. C. Role of Intermolecular Coupling in the Photophysics of Disordered Organic Semiconductors: Aggregate Emission in Regioregular Polythiophene. *Phys. Rev. Lett.* **2007**, *98*, 206406.

(7) Arias, A. C.; MacKenzie, J. D.; Stevenson, R.; Halls, J. J. M.; Inbasekaran, M.; Woo, E. P.; Richards, D.; Friend, R. H. Photovoltaic Performance and Morphology of Polyfluorene Blends: A Combined Microscopic and Photovoltaic Investigation. *Macromolecules* **2001**, *34*, 6005−6013.

(8) Kline, R. J.; McGehee, M. D.; Kadnikova, E. N.; Liu, J.; Fréchet, J. M. J.; Toney, M. F. Dependence of Regioregular Poly(3-Hexylthiophene) Film Morphology and Field-Effect Mobility on Molecular Weight. *Macromolecules* **2005**, *38*, 3312−3319.

(9) Salleo, A.; Kline, R. J.; DeLongchamp, D. M.; Chabinyc, M. L. Microstructural Characterization and Charge Transport in Thin Films of Conjugated Polymers. *Adv. Mater.* **2010**, *22*, 3812−3838.

(10) Groves, C.; Reid, O. G.; Ginger, D. S. Heterogeneity in Polymer Solar Cells: Local Morphology and Performance in Organic Photovoltaics Studied with Scanning Probe Microscopy. *Acc. Chem. Res.* **2010**, *43*, 612−620.

(11) Noriega, R.; Rivnay, J.; Vandewal, K.; Koch, F. P. V.; Stingelin, N.; Smith, P.; Toney, M. F.; Salleo, A. A General Relationship between Disorder, Aggregation and Charge Transport in Conjugated Polymers. *Nat. Mater.* **2013**, *12*, 1038−1044.

(12) Wong, C. Y.; Penwell, S. B.; Cotts, B. L.; Noriega, R.; Wu, H.; Ginsberg, N. S. Revealing Exciton Dynamics in a Small-Molecule Organic Semiconducting Film with Subdomain Transient Absorption Microscopy. *J. Phys. Chem. C* **2013**, *117*, 22111−22122.

(13) Wong, C. Y.; Cotts, B. L.; Wu, H.; Ginsberg, N. S. Exciton Dynamics Reveal Aggregates with Intermolecular Order at Hidden Interfaces in Solution-Cast Organic Semiconducting Films. *Nat. Commun.* **2015**, *6*, 5946.

(14) Bierwagen, J.; Testa, I.; Fölling, J.; Wenzel, D.; Jakobs, S.; Eggeling, C.; Hell, S. W. Far-Field Autofluorescence Nanoscopy. *Nano Lett.* **2010**, *10*, 4249−4252.

(15) Welsh, D. K.; Yoo, S.-H.; Liu, A. C.; Takahashi, J. S.; Kay, S. A. Bioluminescence Imaging of Individual Fibroblasts Reveals Persistent, Independently Phased Circadian Rhythms of Clock Gene Expression. *Curr. Biol.* **2004**, *14*, 2289−2295.

(16) Contag, C. H.; Bachmann, M. H. Advances in in Vivo Bioluminescence Imaging of Gene Expression. *Annu. Rev. Biomed. Eng.* **2002**, *4*, 235−260.

(17) Gustafsson, M. G. L. Nonlinear Structured-Illumination Microscopy: Wide-Field Fluorescence Imaging with Theoretically Unlimited Resolution. *Proc. Natl. Acad. Sci. U. S. A.* **2005**, *102*, 13081−13086.

(18) Betzig, E.; Patterson, G. H.; Sougrat, R.; Lindwasser, O. W.; Olenych, S.; Bonifacino, J. S.; Davidson, M. W.; Lippincott-Schwartz, J.; Hess, H. F. Imaging Intracellular Fluorescent Proteins at Nanometer Resolution. *Science* **2006**, *313*, 1642−1645.

(19) Rust, M. J.; Bates, M.; Zhuang, X. Sub-Diffraction-Limit Imaging by Stochastic Optical Reconstruction Microscopy (STORM). *Nat. Methods* **2006**, *3*, 793−796.

(20) Hess, S. T.; Girirajan, T. P. K.; Mason, M. D. Ultra-High Resolution Imaging by Fluorescence Photoactivation Localization Microscopy. *Biophys. J.* **2006**, *91*, 4258−4272.

(21) Pavani, S. R. P.; Thompson, M. A.; Biteen, J. S.; Lord, S. J.; Liu, N.; Twieg, R. J.; Piestun, R.; Moerner, W. E. Three-Dimensional, Single-Molecule Fluorescence Imaging beyond the Diffraction Limit by Using a Double-Helix Point Spread Function. *Proc. Natl. Acad. Sci. U. S. A.* **2009**, *106*, 2995−2999.

DOI: 10.1021/acs.jpclett.5b01200
J. Phys. Chem. Lett. 2015, 6, 2767−2772

(22) Hell, S. W. Far-Field Optical Nanoscopy. *Science* **2007**, *316*, 1153−1158.
(23) Irvine, S. E.; Staudt, T.; Rittweger, E.; Engelhardt, J.; Hell, S. W. Direct Light-Driven Modulation of Luminescence from Mn-Doped ZnSe Quantum Dots. *Angew. Chem., Int. Ed.* **2008**, *47*, 2685−2688.
(24) Rittweger, E.; Han, K. Y.; Irvine, S. E.; Eggeling, C.; Hell, S. W. STED Microscopy Reveals Crystal Colour Centres with Nanometric Resolution. *Nat. Photonics* **2009**, *3*, 144−147.
(25) Maurer, P. C.; Maze, J. R.; Stanwix, P. L.; Jiang, L.; Gorshkov, A. V.; Zibrov, A. A.; Harke, B.; Hodges, J. S.; Zibrov, A. S.; Yacoby, A. Far-Field Optical Imaging and Manipulation of Individual Spins with Nanoscale Resolution. *Nat. Phys.* **2010**, *6*, 912−918.
(26) Lesoine, M. D.; Bhattacharjee, U.; Guo, Y.; Vela, J.; Petrich, J. W.; Smith, E. A. Subdiffraction, Luminescence-Depletion Imaging of Isolated, Giant, CdSe/CdS Nanocrystal Quantum Dots. *J. Phys. Chem. C* **2013**, *117*, 3662−3667.
(27) Hanne, J.; Falk, H. J.; Görlitz, F.; Hoyer, P.; Engelhardt, J.; Sahl, S. J.; Hell, S. W. STED Nanoscopy with Fluorescent Quantum Dots. *Nat. Commun.* **2015**, *6*, 7127.
(28) Department of NanoBiophotonics; Fluorescent Dyes Used in STED Microscopy. Http://nanobiophotonics.mpibpc.mpg.de/dyes/ (accessed 25 June 2015).
(29) Vogelsang, J.; Steinhauer, C.; Forthmann, C.; Stein, I. H.; Person-Skegro, B.; Cordes, T.; Tinnefeld, P. Make Them Blink: Probes for Super-Resolution Microscopy. *ChemPhysChem* **2010**, *11*, 2475−2490.
(30) Denk, W.; Strickler, J. H.; Webb, W. W. Two-Photon Laser Scanning Fluorescence Microscopy. *Science* **1990**, *248*, 73−76.
(31) Albota, M.; Beljonne, D.; Brédas, J.-L.; Ehrlich, J. E.; Fu, J.-Y.; Heikal, A. A.; Hess, S. E.; Kogej, T.; Levin, M. D.; Marder, S. R. Design of Organic Molecules with Large Two-Photon Absorption Cross Sections. *Science* **1998**, *281*, 1653−1656.
(32) Chemla, D. S. *Nonlinear Optical Properties of Organic Molecules and Crystals*; Elsevier: Amsterdam, 2012.
(33) Scheul, T.; D'Amico, C.; Wang, I.; Vial, J.-C. Two-Photon Excitation and Stimulated Emission Depletion by a Single Wavelength. *Opt. Express* **2011**, *19*, 18036.
(34) Bianchini, P.; Harke, B.; Galiani, S.; Vicidomini, G.; Diaspro, A. Single-Wavelength Two-Photon Excitation−stimulated Emission Depletion (SW2PE-STED) Superresolution Imaging. *Proc. Natl. Acad. Sci. U. S. A.* **2012**, *109*, 6390−6393.
(35) Min, W.; Lu, S.; Chong, S.; Roy, R.; Holtom, G. R.; Xie, X. S. Imaging Chromophores with Undetectable Fluorescence by Stimulated Emission Microscopy. *Nature* **2009**, *461*, 1105−1109.
(36) Wang, P.; Slipchenko, M. N.; Mitchell, J.; Yang, C.; Potma, E. O.; Xu, X.; Cheng, J.-X. Far-Field Imaging of Non-Fluorescent Species with Subdiffraction Resolution. *Nat. Photonics* **2013**, *7*, 449−453.
(37) Szymanski, C.; Wu, C.; Hooper, J.; Salazar, M. A.; Perdomo, A.; Dukes, A.; McNeill, J. Single Molecule Nanoparticles of the Conjugated Polymer MEH−PPV, Preparation and Characterization by Near-Field Scanning Optical Microscopy. *J. Phys. Chem. B* **2005**, *109*, 8543−8546.
(38) Dogariu, A.; Vacar, D.; Heeger, A. J. Picosecond Time-Resolved Spectroscopy of the Excited State in a Soluble Derivative of Poly(phenylene Vinylene): Origin of the Bimolecular Decay. *Phys. Rev. B: Condens. Matter Mater. Phys.* **1998**, *58*, 10218−10224.
(39) Moffitt, J. R.; Osseforth, C.; Michaelis, J. Time-Gating Improves the Spatial Resolution of STED Microscopy. *Opt. Express* **2011**, *19*, 4242.
(40) Vicidomini, G.; Moneron, G.; Han, K. Y.; Westphal, V.; Ta, H.; Reuss, M.; Engelhardt, J.; Eggeling, C.; Hell, S. W. Sharper Low-Power STED Nanoscopy by Time Gating. *Nat. Methods* **2011**, *8*, 571−573.
(41) Dalla Mora, A.; Tosi, A.; Zappa, F.; Cova, S.; Contini, D.; Pifferi, A.; Spinelli, L.; Torricelli, A.; Cubeddu, R. Fast-Gated Single-Photon Avalanche Diode for Wide Dynamic Range Near Infrared Spectroscopy. *IEEE J. Sel. Top. Quantum Electron.* **2010**, *16*, 1023−1030.
(42) Buttafava, M.; Boso, G.; Ruggeri, A.; Mora, A. D.; Tosi, A. Time-Gated Single-Photon Detection Module with 110 Ps Transition Time and up to 80 MHz Repetition Rate. *Rev. Sci. Instrum.* **2014**, *85*, 083114.
(43) Harke, B.; Keller, J.; Ullal, C. K.; Westphal, V.; Schonle, A.; Hell, S. W. Resolution Scaling in STED Microscopy. *Opt. Express* **2008**, *16*, 4154−4162.
(44) Martini, I. B.; Smith, A. D.; Schwartz, B. J. Exciton-Exciton Annihilation and the Production of Interchain Species in Conjugated Polymer Films: Comparing the Ultrafast Stimulated Emission and Photoluminescence Dynamics of MEH-PPV. *Phys. Rev. B: Condens. Matter Mater. Phys.* **2004**, *69*, 035204.
(45) Gaab, K. M.; Bardeen, C. J. Anomalous Exciton Diffusion in the Conjugated Polymer MEH−PPV Measured Using a Three-Pulse Pump−Dump−Probe Anisotropy Experiment. *J. Phys. Chem. A* **2004**, *108*, 10801−10806.
(46) Markov, D. E.; Tanase, C.; Blom, P. W. M.; Wildeman, J. Simultaneous Enhancement of Charge Transport and Exciton Diffusion in Poly(p-Phenylene Vinylene) Derivatives. *Phys. Rev. B: Condens. Matter Mater. Phys.* **2005**, *72*, 045217.
(47) Lewis, A. J.; Ruseckas, A.; Gaudin, O. P. M.; Webster, G. R.; Burn, P. L.; Samuel, I. D. W. Singlet Exciton Diffusion in MEH-PPV Films Studied by Exciton−exciton Annihilation. *Org. Electron.* **2006**, *7*, 452−456.
(48) Akselrod, G. M.; Deotare, P. B.; Thompson, N. J.; Lee, J.; Tisdale, W. A.; Baldo, M. A.; Menon, V. M.; Bulović, V. Visualization of Exciton Transport in Ordered and Disordered Molecular Solids. *Nat. Commun.* **2014**, *5*, 3646.
(49) Akselrod, G. M.; Prins, F.; Poulikakos, L. V.; Lee, E. M. Y.; Weidman, M. C.; Mork, A. J.; Willard, A. P.; Bulović, V.; Tisdale, W. A. Subdiffusive Exciton Transport in Quantum Dot Solids. *Nano Lett.* **2014**, *14*, 3556−3562.
(50) Markov, D. E.; Amsterdam, E.; Blom, P. W. M.; Sieval, A. B.; Hummelen, J. C. Accurate Measurement of the Exciton Diffusion Length in a Conjugated Polymer Using a Heterostructure with a Side-Chain Cross-Linked Fullerene Layer. *J. Phys. Chem. A* **2005**, *109*, 5266−5274.
(51) Lunt, R. R.; Giebink, N. C.; Belak, A. A.; Benziger, J. B.; Forrest, S. R. Exciton Diffusion Lengths of Organic Semiconductor Thin Films Measured by Spectrally Resolved Photoluminescence Quenching. *J. Appl. Phys.* **2009**, *105*, 053711−053711 − 7.
(52) Menke, S. M.; Holmes, R. J. Exciton Diffusion in Organic Photovoltaic Cells. *Energy Environ. Sci.* **2014**, *7*, 499−512.
(53) Lin, J. D. A.; Mikhnenko, O. V.; Chen, J.; Masri, Z.; Ruseckas, A.; Mikhailovsky, A.; Raab, R. P.; Liu, J.; Blom, P. W. M.; Loi, M. A.; et al. Systematic Study of Exciton Diffusion Length in Organic Semiconductors by Six Experimental Methods. *Mater. Horiz.* **2014**, *1*, 280.
(54) Mikhnenko, O.; Blom, P.; Nguyen, T.-Q. T. Exciton Diffusion in Organic Semiconductors. *Energy Environ. Sci.* **2015**, DOI: 10.1039/C5EE00925A.

DOI: 10.1021/acs.jpclett.5b01200
J. Phys. Chem. Lett. 2015, 6, 2767−2772